Talanta 124 (2014) 7–13

Contents lists available at ScienceDirect

Talanta

journal homepage: www.elsevier.com/locate/talanta

Novel monodisperse molecularly imprinted shell for estradiol based on surface imprinted hollow vinyl-SiO_2 particles

Xiaoyan Wang [a,b,c], Qi Kang [a], Dazhong Shen [a,*], Zhong Zhang [b,d], Jinhua Li [b], Lingxin Chen [b,**]

[a] Key Lab in Molecular and Nanomaterials Probes of the Ministry of Education of China, College of Chemistry, Chemical Engineering and Materials Science, Shandong Normal University, Jinan 250014, China
[b] Key Laboratory of Coastal Environmental Processes and Ecological Remediation, Yantai Institute of Coastal Zone Research, Chinese Academy of Sciences, Yantai 264003, China
[c] Binzhou Medical University, Yantai 264003, China
[d] University of Chinese Academy of Sciences, Beijing 100049, China

ARTICLE INFO

Article history:
Received 28 November 2013
Received in revised form
14 February 2014
Accepted 18 February 2014
Available online 25 February 2014

Keywords:
Estradiol
Molecularly imprinted polymer
Surface imprinting
Hollow vinyl-SiO_2 particle
Polystyrene

ABSTRACT

A novel monodisperse molecularly imprinted shell was prepared based on surface imprinted hollow vinyl-SiO_2 particles and applied to selective recognition and adsorption of estradiol (E_2). This method was carried out by introducing vinyltriethoxysilane to the surface of polystyrene (PS) spheres by a simple one-step modification, followed by dissolution to remove the PS cores, and then by copolymerization of functional monomers *via* surface imprinted on the hollow vinyl-SiO_2 particles to prepare uniform E_2-imprinted shells. Two interesting characteristics were found: first, the obtained hollow molecularly imprinted polymer shells (H-MIPs) had highly monodispersity, uniform spherical shape with a shell thickness of about 40 nm; and then, the method was simple, easy to operate by directing coating of a uniform shell on hollow particles *via* surface imprinting. The resultant H-MIPs demonstrated improvements in imprinting factor and binding kinetics, owing to the high selectivity to template molecules, surface imprinting technique and hollow porous structure. Furthermore, satisfactory recoveries of 97.0 and 94.8% with respective precisions of 2.5 and 2.7% were achieved by one-step extraction when H-MIPs were used for the preconcentration and selective separation of estradiol in milk samples at two spiked levels. The simple, effective H-MIPs based strategy provided new insights into the formation of various functionalized coating layers on different kinds of support materials with versatile potential applications.

1. Introduction

During recent years, it has been increasingly reported that endocrine disrupting compounds (EDCs) enter the human living environment. These compounds have become a growing concern due to their potential in altering the normal endocrine function and physiological status of humans and animals [1]. Estradiol (17β-Estradiol or E_2), as the most active estrogen, can disrupt vital systems (*e.g.*, the endocrine system) in aquatic organisms and increase the risk of cancer [2,3]. In order to prevent the uncontrolled effects on the human health and the deleterious effects on the aquatic environment, the development of highly effective and practicable methods for the selective recognition, determination and removal of trace residues of E_2 is urgently required.

Molecularly imprinting is known as a technique for the generation of polymer-based molecular recognition elements tailor-made for a given target or a group of target molecules [4–6]. The resulting molecularly imprinted polymers (MIPs) not only possess desired binding properties, selectivity and specificity for target molecules, but also exhibit far greater physical robustness and thermal stability. These characteristics allow MIPs to be used in a wide range of fields, such as separation, sensors, catalysis and drug delivery [7–11]. However, the MIPs prepared by traditional methods have met with many limitations including incomplete template removal, small binding capacity, low affinity, and irregular materials' shape. One of main reasons is that the removal of template molecules located at interior area of bulk materials is quite difficult due to the high cross-linking nature of MIPs [12]. Recently, the synthesis of core–shell-type MIPs has provided a convenient and controllable approach for preparing MIPs, due to

* Corresponding author. Tel.: +86 531 86180740; fax: +86 531 82615258.
** Corresponding author. Tel./fax: +86 535 2109130.
E-mail addresses: dzshen@sdnu.edu.cn (D. Shen), lxchen@yic.ac.cn (L. Chen).

http://dx.doi.org/10.1016/j.talanta.2014.02.040
0039-9140

its intrinsic advantages, such as good dispersion, rapid binding kinetics, easy and complete removal of template molecules [13–15]. Monomer-directing polymerization [12] and layer-by-layer deposition [16] protocols for highly dense imprinting of 2,4,6-trinitrotoluene on the surface of silica nanoparticles are developed. These techniques have been widely adopted for producing core–shell MIP microspheres. Although the method to obtain core–shell imprinted microspheres possesses remarkable advantages, the resultant products often have a low rebinding capacity [17], since the solid cores do not generate recognition cavities and possess most mass of the imprinted materials, which decreases the binding capacity per unit mass of MIPs.

To solve these problems, recently, our group has begun to explore alternative approaches by combining molecular imprinting technology with hollow polymer preparation methods [18,19]. Several types of hollow porous MIPs were prepared by multistep seed swelling polymerization, and were applied as solid-phase extraction sorbents for selective preconcentration and specific recognition of triazines in soil samples [18] and Sudan I in chilli sauce samples [19]. The main advantages recognized up to now in the use of hollow polymers can be attributed to their controllable pore and hole structures, which favors mass transfer.

Inspired by these studies, now, we aspired to extend the hollow molecularly imprinting polymer preparation methods to the direct coating of a uniform shell on hollow particles *via* surface imprinting. Vinyltriethoxysilane (VTES) as a precursor was first introduced to the surface of polystyrene (PS) spheres by a simple one-step modification, followed by dissolution to remove the PS cores, and thus by copolymerization of functional monomers on hollow vinyl-SiO_2 particles to prepare uniform E_2-imprinted polymer shells. The developed approach could supply great application potentials not only in molecular imprinting fields, but also in the preparation of various functional coating layers on PS support.

2. Experimental

2.1. Materials and instruments

2-(Methacryloyl)ethyl trimethylammonium chloride (MTC) aqueous solution, vinyltriethoxysilane (VTES), E_2, estriol (E_3), diethylstilbestrol (DES), methacrylic acid (MAA), and ethyleneglycol dimethacrylate (EGDMA) were purchased from Sigma-Aldrich and used as received. Styrene (St) was purchased from Sigma-Aldrich and purified by washing with NaOH and ultrapure water. 2,2′-Azobis-isobutyronitrile (AIBN) was obtained from Shanghai Chemical Reagents Company (Shanghai, China) and recrystallized in methanol prior to use. Polyvinylpyrrolidone (PVP), tetrahydrofuran (THF), and aqueous ammonia solution were supplied by Tianjin Reagent Plant (Tianjin, China). High performance liquid chromatography (HPLC) grade acetonitrile (ACN) was purchased from Merck (Darmstadt, Germany). Deionized water used throughout the work was produced by a Milli-Q Ultrapure water system with the water outlet operating at 18.2 MΩ (Millipore, Bedford, MA, USA).

FT-IR analyses were carried out by a FT-IR spectrometer (Thermo Nicolet Corporation, USA). The morphological evaluation was observed by TEM (JEM-1230, operating at 100 kV) and SEM (JSM 5600 LV, operating at 20 kV). The specific surface areas and pore sizes of the polymers were measured *via* Brunauer–Emmett–Teller (BET) analysis by nitrogen adsorption experiments. The measurement was operated on AUTOSORB 1 (Quantachrome Instruments, Germany). The samples were degassed at 250 °C in vacuum prior to adsorption measurements. Thermogravimetric (TG) analysis about thermostability and purity was performed by a ZRY-2P thermal analyzer (Mettler Toledo).

2.2. Preparation of PS support particles

The monodisperse positively charged PS particles were prepared by dispersion polymerization as described [20] with necessary modifications. Briefly, 6 mL St, 1.5 g PVP, 0.2 g AIBN, 5 mL H_2O and 29 mL ethanol were charged into a 250 mL three-necked flask. The mixing solution was deoxygenated by bubbling nitrogen gas at room temperature for 30 min, and was then heated to 70 °C with vigorous magnetic stirring for 1.5 h, followed by addition of 6 mL St, 29 mL ethanol and 0.39 g MTC. Then the reaction was carried out under vigorous magnetic stirring at 70 °C for 24 h.

2.3. Synthesis of hollow vinyl-SiO_2 spheres

The obtained PS suspension was cooled to 50 °C, and 3 mL ammonia was then added and the mixture was stirred for 5 min. 9 g VTES was added dropwise to the suspension and the mixture reacted at 50 °C for around 5 h with constant stirring. The monodisperse PS@vinyl-SiO_2 core–shell particles were obtained. Then the particles were separated from the reaction medium by centrifuging, and then were washed several times with ethanol. After removing the PS cores by dissolution in THF, the hollow vinyl-SiO_2 spheres were attained.

2.4. Molecular imprinting on the surface of hollow vinyl-SiO_2 spheres

Typically, hollow vinyl-SiO_2 spheres (50 mg) were dispersed in 50 mL of ACN by ultrasonication. E_2 (68 mg, 0.25 mmol), MAA (85 μL, 1 mmol), EGDMA (945 μL, 5 mmol) and AIBN (20 mg) were then added into the above solution followed by purging with nitrogen for 30 min. A two-step temperature-rising polymerization reaction was carried out in a water bath at 50 °C for 8 h, followed by 60 °C for 24 h. The resultant polymer shells were separated and washed with methanol/acetic acid solution (9:1, v/v) to remove both the template molecules and residual monomers. Finally, the polymer shells were dried to constant weight under vacuum at 40 °C. For comparison, solid molecularly imprinted polymers were prepared in the same manner but without removing the PS cores, namely S-MIPs for simplicity. As a control, their corresponding non-imprinted polymers (NIPs) were prepared under identical conditions but omitting the template in the reaction system.

2.5. Adsorption property investigation of the H-MIPs

The adsorption experiments were carried out as follows: 20 mg polymers were dispersed in a 5 mL flask containing 2.0 mL E_2 solutions of various concentrations. After 24 h of shaking at room temperature, the samples were centrifuged. The amount of E_2 adsorbed onto the imprinted polymer shells was determined by measuring the difference between total E_2 amount and residual amount in solution with HPLC-UV. Meanwhile, the binding kinetics was detected by monitoring the temporal amount of E_2 in the solutions at regular times. Selectivity experiments were made by using E_3 and DES as structural analogs.

2.6. Analysis of E_2 in milk samples

The milk samples analyzed were obtained from local markets. 30 mL ACN was added to 10 mL of milk sample and the mixture was shaken vigorously for 15 min. Thereafter, the mixture was centrifuged at 4500 rpm for 30 min. For spiked tests, appropriate amounts of E_2 standard were added into the milk sample and extracted from the matrix through the overall procedure, at levels of 10 and 100 $\mu g\,L^{-1}$, respectively. H-MIPs of 100 mg were dispersed in 5 mL blank or spiked solutions and incubated for

1 h at room temperature before being collected using a 0.22 μm microporous membrane. The H-MIPs were washed with 3 mL methanol to reduce nonspecific adsorption, and then eluted with 5 mL desorption solvent of methanol/acetic acid (9:1, v/v). The resultant solution was dried and redissolved in 200 μL ACN and then analyzed by HPLC. HPLC analysis was performed using a C_{18} column (Arcus EP-C_{18}, 5 μm, 4.6 × 250 mm Column, Exformma Technologies, USA) as the analytical column. HPLC conditions were as follows: mobile phase, ACN/water (70:30, v/v); flow rate, 1.0 mL min^{-1}; room temperature; UV detection at 280 nm; injection volume, 20 μL.

3. Results and discussion

3.1. Preparation of H-MIPs

Core–shell type MIP microspheres are particularly interesting because they provide a convenient and controllable approach for preparing MIP microspheres. Furthermore, they possess two remarkable advantages over traditionally imprinted materials [15]. The first concern is surface imprinting on colloidal spheres providing easy and complete removal of template molecules, and excellent accessibility to target species. The second one is that core–shell architecture is a feasible way to combine multiple functionalities (*e.g.*, magnetic, fluorescent) into MIPs because the core is independent of the shell. However, the area of core–shell MIPs surface is greatly limited, and the solid cores in core–shell imprinted microspheres are unavailable for template recognition, thus lowering the rebinding capacity of MIPs. In order to obtain high binding capacity per unit mass of MIPs, molecularly imprinting polymer shells were proposed in the present work. The preparation process of the polymer shells is schematically illustrated in Fig. 1. In the first step, vinyl groups were introduced to the surface of PS particles through chemical modification with VTES, following with the removal of PS cores for facilitating copolymerization with functional monomers. Then the hollow vinyl-SiO_2 particles were suspended in ACN solutions containing functional monomer (MAA), crosslinker (EGDMA), template (E_2), and initiator (AIBN). Herein, a two-step temperature-rising polymerization was used in order to form a uniform shell. A thin oligomer layer could form at the surface of hollow vinyl-SiO_2 particles at lower temperature, which would induce the following polymerization to occur at the surface of the hollow vinyl-SiO_2 particles. At higher temperature, the polymerization proceeded fast, and then the shell was mainly obtained during this process, and finally, recognition sites located at the surface of the polymer shells were attained after removal of the template molecules.

The monodisperse PS particles were prepared by dispersion polymerization. The vinyl-functionalized SiO_2 was coated on the surface of PS core following a modified Stöber process that

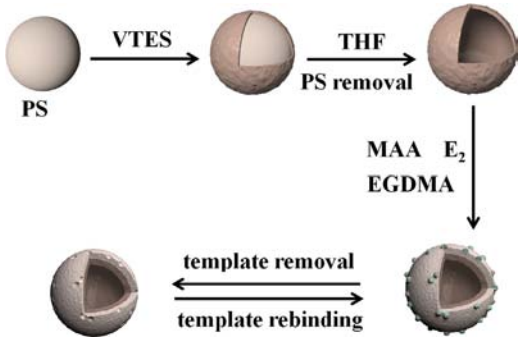

Fig. 1. Preparation process of the H-MIPs.

involved the hydrolysis of VTES in aqueous solution [21]. After removing the PS cores by dissolution in THF, the hollow vinyl-SiO_2 spheres were obtained. The TEM image of the obtained PS particles was shown in Fig. 2A, and it can be seen that uniform spherical PS particles with an average diameter of 1 μm were highly monodisperse and the surface was quite smooth, which provided the opportunity to obtain good morphological vinyl functionalized core–shell silica spheres, indicated by Fig. 2B. As seen from the TEM image of Fig. 2C and SEM image of Fig. 2E, the hollow vinyl-SiO_2 spheres with a shell thickness about 20 nm were still well monodisperse and spherical. Furthermore, excitedly, a uniform molecularly imprinting layer microsphere was formed, by coating at the surface of hollow vinyl-SiO_2 particles, as seen from Fig. 2D and F, with an imprinting shell thickness of about 40 nm.

Actually, the concentrations of polymerization precursors such as functional monomers and cross-linkers have an important effect on the effectiveness of the imprinted shell. The conditions were investigated as follows. The hollow vinyl-SiO_2 spheres (50 mg) were dispersed in 50 mL of ACN. Increasing the polymerization precursors to double (the mole ratio of MAA to EGDMA was consistently 1:4) would result in the formation of homogeneous self-polymerization of monomers and secondary particles with the size of 300 nm (Fig. S1B). When keeping the amount of polymerization precursors constant, increasing the amount of hollow vinyl-SiO_2 spheres from 50 to 100 mg in surface imprinting, hollow vinyl-SiO_2 spheres could not be monodisperse in the solution, which would lead to the aggregation of imprinted polymers (Fig. S1C). So, the ideal imprinting microspheres were obtained with imprinting shell thickness of 40 nm, as observed in Fig. 2D and F, when 1 mmol MAA (85 μL), 5 mmol EGDMA (945 μL) and 50 mg hollow vinyl-SiO_2 spheres were used.

3.2. Characterization of the H-MIPs

Fig. 3 shows the N_2 adsorption–desorption isotherms and pore size distribution of H-MIPs and H-NIPs. As seen from Fig. 3A, when the relative pressure P/P_0 was less than 0.8, the slope of the curves was very small, and this indicated that very little amount of small size pores existed on the surface of H-MIPs. In contrast, when the relative pressure P/P_0 was higher than 0.8, the slope of the curves increased sharply. As observed, the desorption curve was closer but leveled above the adsorption curve, which could be the evidence of a small quantity of micropores present on shell of the H-MIPs [22]. The narrow pore diameter distribution and low average pore diameter displayed from the adsorption plot, as shown from Fig. 3B, suggested that the size of the cavities formed in the H-MIPs played a key role in binding capacity. Related morphological structure parameters of H-MIPs and H-NIPs are listed in Table 1. As seen, the specific surface area (161.2 $m^2 g^{-1}$) and cumulative pore volume (0.816 mL g^{-1}) of H-MIPs were much larger than those of H-NIPs. The results indicated the H-MIPs have uniform regular spherical structure. The large cumulative pore volume is very likely owing to the microspores on the surface of H-MIPs, which revealed that the template E_2 molecules were almost completely eluted and removed and thereby leading to considerable amounts of imprinting cavity sites.

Fig. 4 shows the FT-IR spectra of hollow vinyl-SiO_2 spheres (a) and H-MIPs (b). The peaks at 1132 and 1045 cm^{-1} could be attributed to Si–O–Si asymmetric stretching. The absorption peak at 3435 cm^{-1} belongs to Si–OH stretching vibration [23]. The characteristic peaks of PS at 758, 698, 1452, 1493, 1603, 3061 and 3026 cm^{-1} [24] illustrated a small quantity of PS remained in hollow vinyl-SiO_2 spheres. However, vinyl groups existing in the hollow vinyl-SiO_2 spheres were identified, due to the $-CH_2$ in-plane bending deformation observed at nearly 1410 cm^{-1} which was in combination with C=C stretching at about 1603 cm^{-1}. The

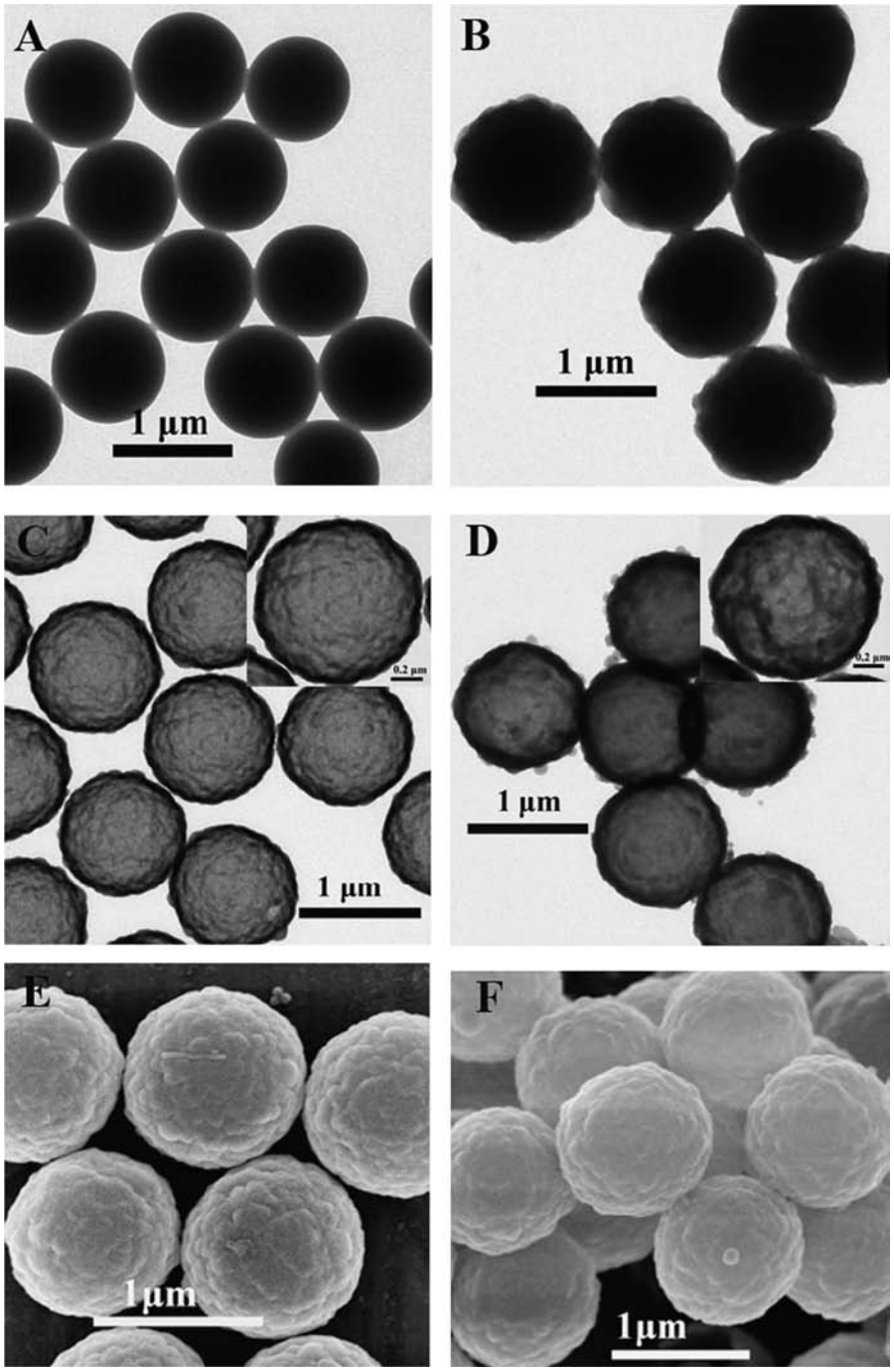

Fig. 2. TEM images of (A) PS particles, (B) vinyl functionalized silica spheres, (C) vinyl functionalized hollow silica spheres, (D) E_2-imprinted H-MIPs, and the inset in (C) and (D) is a high-magnification TEM image (Scale bar=0.2 μm). SEM images of (E) vinyl functionalized hollow silica spheres and (F) E_2-imprinted H-MIPs.

results indicated that hollow vinyl-SiO_2 spheres had been successfully prepared. FT-IR spectrum of H-MIPs has the characteristic peaks of carbonyl groups at 1731 cm^{-1}, which verified the successful introduction of the functional groups in the imprinted cavities.

Fig. 5 shows the TG curves of PS, hollow vinyl-SiO_2, and H-MIPs. The PS particles were fully decomposed after calcinations. The hollow vinyl-SiO_2 spheres showed an initial weight increase and then a loss. The adsorption of nitrogen probably caused the weight increase, and the later weight loss could be ascribed to the degradation of organic parts [21]. The final residue was 32.8%. The H-MIPs had a similar TG curve, exhibiting an initial weight increase and then a loss. A higher rate of weight loss was presented at temperatures ranging from 390 to 490 °C, and the corresponding residual amounts were 72.7%. The weight loss might result from the dissolving of MIPs [19]. Hence, the prepared H-MIPs could keep good thermal stability below 390 °C.

3.3. Binding property investigation of the H-MIPs

In order to investigate the molecular recognition properties of the E_2 imprinted polymer shells, static, dynamic and selective binding experiments were carried out. As shown in Fig. 6A, the binding capacity of H-MIPs increased quickly and continuously along with the increase of initial concentration. As seen, the maximum adsorption capacity of the H-MIPs was approximately

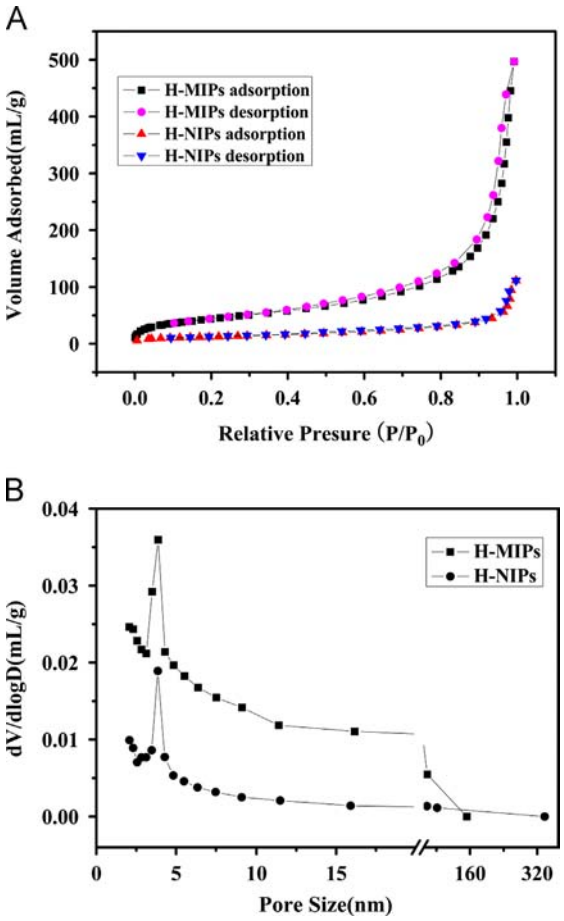

Fig. 3. (A) N_2 adsorption–desorption isotherms and (B) pore size distribution of H-MIPs and H-NIPs.

Table 1
Specific surface area and other related data of H-MIPs and H-NIPs obtained by BET analysis.

Polymer	Specific surface area ($m^2\,g^{-1}$)	Cumulative pore volume ($mL\,g^{-1}$)	Average pore diameter (nm)	Cumulative pore area ($m^2\,g^{-1}$)
H-MIPs	161.2	0.816	14.8	220.4
H-NIPs	44.3	0.181	12.9	55.9

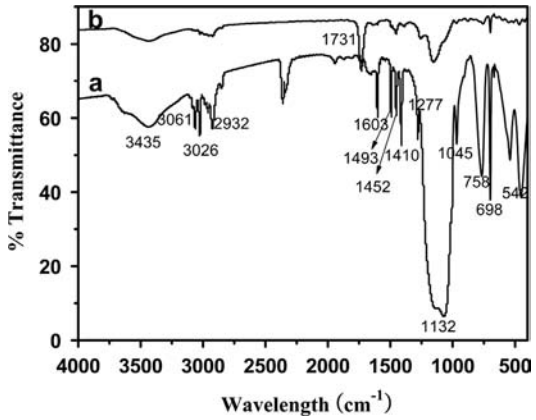

Fig. 4. FT-IR spectra of (a) vinyl functionalized hollow silica spheres and (b) H-MIPs.

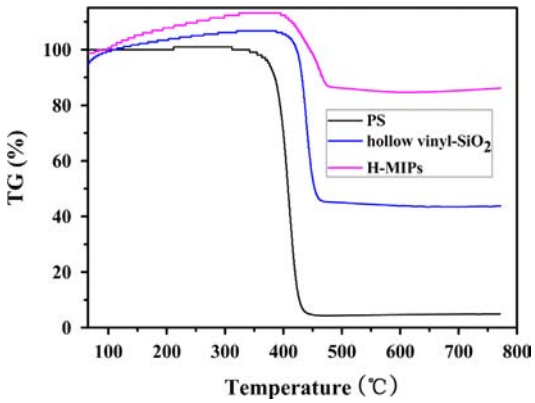

Fig. 5. TG curves of PS, hollow vinyl-SiO_2 and H-MIPs.

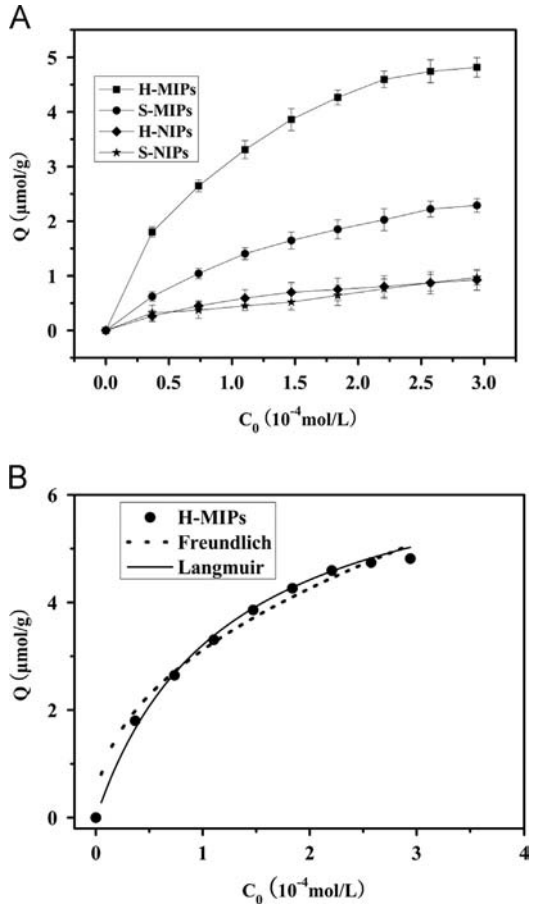

Fig. 6. (A) Binding isotherms of H-MIPs, S-MIPs and their corresponding NIPs for E_2 in acetonitrile. Q, adsorption capacity; C_0, initial concentration of E_2. Experimental conditions: V=2.0 mL; mass of polymers, 20 mg; adsorption time, 24 h. (B) Comparison of Langmuir and Freundlich isotherm models for E_2 adsorption onto H-MIPs.

4.82 μmol/g, whereas that of the corresponding H-NIPs was only about 0.92 μmol/g. This could be attributed to the larger specific surface area and cumulative pore volume of the H-MIPs. Meanwhile, it was found the adsorption capacity of the H-MIPs was also much higher than that of the S-MIPs (Fig. 6A), which suggested the hollow imprinted microspheres not only generated more recognition cavities on the imprinted shell, but also increased the adsorption capacity per unit mass of MIPs. Moreover, a high imprinting factor for the H-MIPs was attained of 5.2. All these results revealed that the adsorption was highly specific for surface imprinted sites in shells owing to high monodispersity, uniform

spherical shape with a thickness of about 40 nm, which ensured the complete removal of templates and good accessibility of target molecules.

On the other hand, it should be noted that the maximum binding capacity value of 4.82 μmol/g for the H-MIPs was not very high. As is well known, an appropriate shell thickness is critical to achieve the maximum binding capacity. In addition, low amounts of polymerization precursors, including functional monomers and cross-linkers, used in polymerization lead to thinner shell, which is beneficial for monodispersity, uniform spherical shape and complete template removal, and thereby improving the accessibility of the binding sites, allowing all of the recognition sites to be used. However, thin shell usually results in low binding capacity. On the other hand, further increasing the polymerization precursors will cause self-polymerization of monomers, incomplete template removal and aggregation of imprinted nanoparticles. Therefore, greater development potential is highly expected and more efforts should be made to further improve the binding capacities and imprinting performances of hollow MIPs.

In order to optimize the design of an adsorption system to separate E_2 from solutions, it is important to establish the most appropriate correlation for the equilibrium curve. Theoretically, the adsorption capacity at equilibrium is commonly expressed by an adsorption isotherm. Equilibrium data in this study were analyzed with two common isotherm models: Langmuir and Freundlich isotherm models [25]. Equilibrium data for Freundlich and Langmuir isotherms for adsorption of E_2 onto H-MIPs was displayed in Fig. 6B. It can be seen that the Langmuir isotherm model is quite suitable to the adsorption. The isotherm parameters obtained from linear analysis are presented in Table 2. It is also confirmed that the Langmuir isotherm model displayed a better fit than that by the Freundlich model, for the correlation coefficients (R^2) above 0.99.

Scatchard analysis was employed to further analyze the molecular recognition properties of imprinted polymer shells. The Scatchard equation is expressed as the following Eq. (1) [25]:

$$\frac{Q_e}{c} = \frac{Q_{max}}{K_d} - \frac{Q_e}{K_d} \quad (1)$$

where Q_e is the amount adsorbed at equilibrium, c is the free concentration at equilibrium, K_d is the dissociation constant, and Q_{max} is the apparent maximum amount that can be bound. K_d and Q_{max} can be calculated from the slope and intercept of the linear curve plotted in Q_e/c vs. Q_e. For H-MIPs, K_d and Q_{max} were estimated to be 0.113 mmol L^{-1} and 6.87 μmol, respectively, whereas the values for H-NIPs were 0.141 mmol L^{-1} and 1.57 μmol, respectively, which was consistent with the experimental results.

Fig. 7 shows the time-dependent increase in the amount of E_2 bound by H-MIPs and H-NIPs. Before the dynamic adsorption equilibrium was reached, the H-MIPs took up E_2 molecules from the solution phase at a fast rate. The H-MIPs spent the equilibrium time period shorter than 60 min. Meanwhile, the H-NIPs needed longer than 90 min to reach the equilibrium period. This phenomenon could find answers from the TEM/SEM images of Fig. 2 and nitrogen adsorption–desorption results of Fig. 3. Depending on the ideal pore sizes, E_2 could easily move into or away the recognition sites of H-MIPs. As a result, the H-MIPs occupied higher binding capacity and faster mass transfer.

To further evaluate the competitive recognition ability of the polymer shells, two estrogen compounds with similar structure and characteristics such as E_3 and DES were used. It can be seen from Fig. 8 that H-MIPs exhibited good adsorption selectivity for the template molecule E_2. However, the H-NIPs exhibited inconspicuous difference among E_2, E_3 and DES. The adsorption capacity of H-MIPs to E_2 were about 1.2 and 3.5 times that of E_3 and DES. The reason can be explained as follows: the binding capacities for E_3 were higher than DES, as its similar size, shape and action sites to E_2. In addition, H-MIPs displayed the poor affinity to DES, the

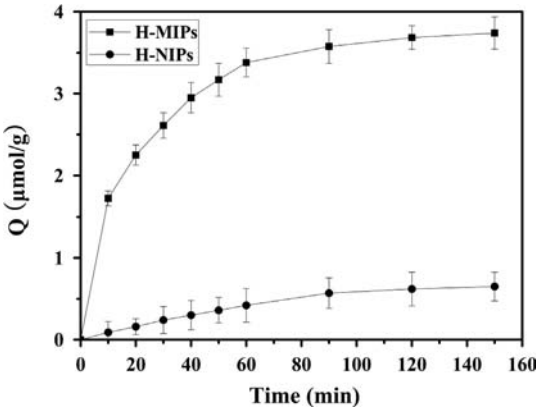

Fig. 7. Kinetic uptake of E_2 molecules onto H-MIPs and H-NIPs. Experimental conditions: V=2.0 mL, C_0=40 mg L^{-1}, mass of polymers, 20 mg.

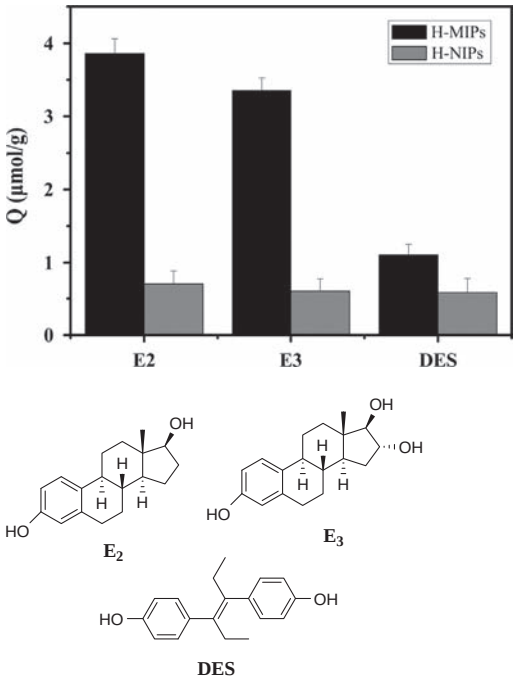

Fig. 8. Binding capacities of H-MIPs and H-NIPs for E_2, E_3 and DES, and their chemical structures. The conditions for the measurements were as follows: mass of polymers, 20 mg; initial concentration of the compounds, 40 mg L^{-1}; V=2.0 mL; adsorption time, 24 h; room temperature.

Table 2
Langmuir and Freundlich isotherm model parameters for the H-MIPs and H-NIPs.

Isotherm model	Parameters	H-MIPs	H-NIPs
Langmuir	R^2[a]	0.996	0.998
	Q_{max}[b]	7.09	1.33
	K_L[c]	0.828	0.712
Freundlich	R^2	0.979	0.982
	K_F[d]	3.12	0.534
	$1/n$[e]	0.451	0.529

[a] Correlation coefficient.
[b] Maximum binding capacity.
[c] Langmuir constant.
[d] Indicative constant for adsorption capacity of the adsorbent.
[e] Ranging from 0 to 1, measuring the adsorption intensity or surface heterogeneity.

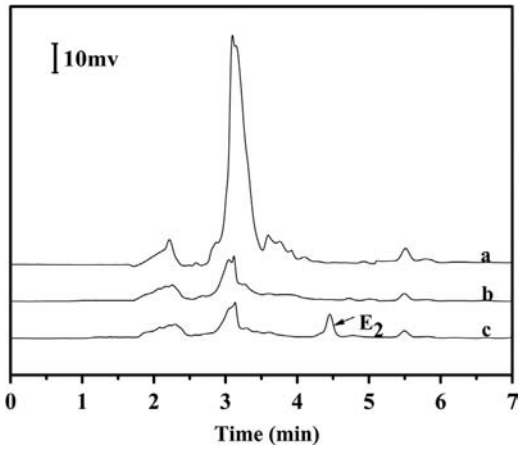

Fig. 9. HPLC-UV chromatograms of milk samples: (a) without extraction; extraction with H-MIPs without spiking (b) and spiked with 100 μg L^{-1} E_2 standard (c).

main reason might be that DES molecules had different structure and inappropriate size to E_2, which were hard to be adsorbed in the specific binding sites. These comparisons clearly demonstrated that the H-MIPs had high selectivity for the target species. So, the obtained MIPs could selectively recognize the delicate difference of E_2 from its analogs.

3.4. Applications of the H-MIPs to milk sample analysis

To evaluate the practical applicability of the H-MIPs to selective separation of E_2, the spiked milk samples were analyzed. High recoveries of 97.0 and 94.8% with the corresponding relative standard deviations (RSD) of 2.5 and 2.7% were obtained for the spiked E_2 at 10 and 100 μg L^{-1}, respectively. The results demonstrated that the H-MIPs were potentially applicable for highly effective preconcentration, separation and accurate quantification of E_2 in real samples. Fig. 9 shows the chromatograms of E_2 from milk samples. As seen from Fig. 9a, the endogenous E_2 was not detected, and it was quite difficult to detect E_2 without performing the extraction process since the targeted E_2 is usually present at low concentration level and complicated matrices usually show severe interferences. Excitedly, after extraction by H-MIPs, the matrix effects were drastically reduced (Fig. 9b and c), and the spiked E_2 was remarkably concentrated as shown in Fig. 9c, which could be attributed to the fact that the H-MIPs had a highly selective recognition and enrichment ability. In the milk sample, favorable limit of detection (LOD, $S/N=3$) and limit of quantitation (LOQ, $S/N=10$) by using H-MIPs were attained of 4.6 and 15.3 μg L^{-1}, respectively. Hence, the H-MIPs offered a simple and high-efficiency enrichment strategy for trace E_2 from complicated matrices.

4. Conclusions

A facile and general approach was developed for the synthesis of a novel monodisperse molecularly imprinted shell by surface imprinting of hollow vinyl-SiO_2 for selective recognition and enrichment of E_2. The resultant polymer shells exhibited excellent characteristics, such as high imprinting factor and fast binding kinetics towards E_2 owing to the hollow structure with the specific adsorption to target molecules and low mass transfer resistance. Langmuir model was well fitted with the static adsorption data and indicated the formation of monolayer coverage of E_2 at the surface of the molecularly imprinted polymer shells. In addition, the developed method based on molecularly imprinted polymer shells was successfully applied to E_2 analysis in spiked milk samples with high recoveries and precisions. Furthermore, the hollow imprinted microspheres had a mean diameter of about 1 μm, and, thus, could be employed as highly selective packing sorbents for HPLC columns. Besides, molecularly imprinting combined with hollow particles opens a new window of interest in the exploration of functionalized polymer shells, as well as provides new opportunities in the applications to recognition, determination and removal of trace targeted species from complicated matrices.

Acknowledgments

The authors gratefully acknowledge financial supports of the National Natural Science Foundation of China (21175084, 21275091, 21105117), the Research Fund for the Doctoral Program of Higher Education of China (20113704110003) and the 100 Talents Program of the Chinese Academy of Sciences.

Appendix A. Supplementary material

Supplementary data associated with this article can be found in the online version at http://dx.doi.org/10.1016/j.talanta.2014.02.040.

References

[1] K.E. Tollefsen, J.F.A. Meys, J. Frydenlund, J. Stenersen, Mar. Environ. Res. 54 (2002) 697–701.
[2] R. Lange, T.H. Hutchinson, C.P. Croudace, F. Siegmund, H. Schweinfurth, P. Hampe, Environ. Toxicol. Chem. 20 (2001) 1216–1227.
[3] S.C. Kang, B.M. Lee, J. Toxicol. Environ. Health A 68 (2005) 1833–1840.
[4] X. Wang, L.Y. Wang, X.W. He, Y.K. Zhang, L.X. Chen, Talanta 78 (2009) 327–332.
[5] L.X. Chen, S.F. Xu, J.H. Li, Chem. Soc. Rev. 40 (2011) 2922–2942.
[6] S.F. Xu, H.Z. Lu, X.W. Zheng, L.X. Chen, J. Mater. Chem. C 1 (2013) 4406–4422.
[7] X.L. Song, J.H. Li, S.F. Xu, R.J. Ying, J.P. Ma, C.Y. Liao, D.Y. Liu, J.B. Yu, L.X. Chen, Talanta 99 (2012) 75–82.
[8] X.Q. Cai, J.H. Li, Z. Zhang, F.F. Yang, R.C. Dong, L.X. Chen, ACS Appl. Mater. Interfaces 6 (2014) 305–313.
[9] J.H. Li, Z. Zhang, S.F. Xu, H. Xiong, H.L. Peng, N. Zhou, L.X. Chen, J. Mater. Chem. 21 (2011) 19267–19274.
[10] E.A. Karakhanov, A.L. Maximov, Curr. Org. Chem. 14 (2010) 1284–1295.
[11] D.A. Spivak, Adv. Drug Deliv. Rev. 57 (2005) 1779–1794.
[12] D.M. Gao, Z.P. Zhang, M.H. Wu, C.G. Xie, G.J. Guan, D.P. Wang, J. Am. Chem. Soc. 129 (2007) 7859–7866.
[13] C.J. Tan, H.G. Chua, K.H. Ker, Y.W. Tong, Anal. Chem. 80 (2008) 683–692.
[14] C.J. Tan, Y.W. Tong, Anal. Chem. 79 (2007) 299–306.
[15] G.J. Guan, R.Y. Liu, Q.S. Mei, Z.P. Zhang, Chem. Eur. J. 18 (2012) 4692–4698.
[16] G.J. Guan, R.Y. Liu, M.H. Wu, Z. Li, B.H. Liu, Z.Y. Wang, D.M. Gao, Z.P. Zhang, Analyst 134 (2009) 1880–1886.
[17] A. Bossi, S.A. Piletsky, E.V. Piletska, P.G. Righetti, A.P.F. Turner, Anal. Chem. 73 (2001) 5281–5286.
[18] S.F. Xu, L.X. Chen, J.H. Li, W. Qin, J.P. Ma, J. Mater. Chem. 21 (2011) 12047–12053.
[19] Z. Zhang, S.F. Xu, J.H. Li, H. Xiong, H.L. Peng, L.X. Chen, J. Agric. Food Chem. 60 (2012) 180–187.
[20] M. Chen, L.M. Wu, S.X. Zhou, B. You, Adv. Mater. 18 (2006) 801–806.
[21] T.S. Deng, F. Marlow, Chem. Mater. 24 (2012) 536–542.
[22] J.J. Yuan, D.C. Wan, Z.L. Yang, J. Phys. Chem. C 112 (2008) 17156–17160.
[23] D.L. Ou, A.B. Seddon, J. Non-Cryst. Solids 210 (1997) 187–203.
[24] J.C. Tang, G.W. Li, R.F. Zhang, J.C. Shen, J. Mater. Chem. 13 (2003) 232–234.
[25] W.L. Guo, W. Hu, J.M. Pan, H.C. Zhou, W. Guan, X. Wang, J.D. Dai, L.C. Xu, Chem. Eng. J. 171 (2011) 603–611.